Nanoscale deconfinement driven faster dynamics of hydrated RNA on a Nanodiamond surface

Gurpreet K. Dhindsa[1], Debsindhu Bhowmik[1], Monojoy Goswami[2,3], Vadym N. Mochalin[4*], Hugh O'Neill[5], Yury Gogotsi[4], Eugene Mamontov[6], Bobby G. Sumpter[2,3] Liang Hong[7],Panchapakesan Ganesh[2*] and Xiang-qiang Chu[1*]*

[1]Dept. of Physics and Astronomy, Wayne State University USA; [2]Center for Nanophase Materials Sciences, Oak Ridge National Laboratory; [3]Computer Science and Mathematics Division, Oak Ridge National Laboratory;4 Department of Chemistry, Missouri University of Science & Technology, Rolla, USA; [4]Drexel University, Philadelphia, USA; [5]Biology and Soft Matter Division, Oak Ridge National Laboratory, USA; [6]SNS Oak Ridge National Laboratory, USA; [6]Institute of Natural Science, Shanghai Jiao Tong University

*ganeshp@ornl.gov, *goswamim@ornl.gov, *chux@wayne.edu, mochalinv@mst.edu

Abstract

Nanodiamonds (ND) have recently been considered as potential vehicles for biomolecular drug delivery due to their non-cytotoxicity and biocompatibility. However, a detailed elucidation of the interfaces between the ND, water, and biomolecules is required to understand how the hydrophilic ND surface fundamentally alters the structure and dynamics of hydrated biomolecules. We report a combined neutron scattering and molecular dynamics study of the water/RNA/ND system. We discover that the RNA molecules on a ND surface demonstrate significantly enhanced dynamics contrary to the generally regarded notion of slower dynamics at the interface. The surprisingly faster motion is driven by a decoupling of RNA and water dynamics due to weaker dynamic heterogeneity on the hydrophilic ND surface, a consequence of deconfinement of RNA molecules. This new finding deepens our understanding of interfacial layers forming a corona on nanoparticles in biofluids, thereby suggesting new design principles for improved and safer drug delivery platforms.

Introduction

Billions of years of natural evolution has created a set of functional building-block molecules like RNA and DNA[1] that enable various fundamental biological functions. Humankind, on the other hand, is no less creative in rivaling the biological complexity while producing materials like nanodiamonds that can have ramifications for biomedical applications[2]. DNA based nanomaterials are now well established[3] in nanomechanical devices and drug delivery applications[4]. Similarly, there is a surge in interest in RNA nanotechnology in recent years due to its potential applications in the treatment of cancer and genetic disorders[1]. On the carbon-based

nanomaterials front, nanodiamond (ND) is considered a viable candidate for drug delivery in lung carcinoma cells[5] and bactericidal applications[6] due to its low cytotoxicity and higher biocompatibility. ND is an excellent platform because of the robust structure and tailorable surface chemistry. Due to its consistent nearly spherical shape, ND is also safer compared to tubular shaped nanomaterials[7]. Functionalized ND complexed with biodegradable, biocompatible polymers has recently been demonstrated for biomedical applications[8]. Since the surface of ND can be easily tailored by termination with hydrophilic groups (ether-C-O-C, peroxide –C-O-O-, carbonyl –C=O, carboxyl COOH, hydroxyl O-H, etc.) and hydrocarbon fragments to adsorb and covalently attach large number of biologically active molecules[9], including triple-helical peptides with wound-healing activity, it is prudent to pursue RNA-ND system as possible platform for gene silencing therapy. Besides drug delivery NDs have been shown to be well suited for applications in tissue engineering[1,10], tribology[2] and bio-imaging[2,11]. However there is very little understanding of the structure as well as dynamics of biomolecules adsorbed on ND. Biomolecules are quickly adsorbed from the environment surrounding ND onto its surface, so called "corona effect", known for nanoparticles in general. The "corona" of biomolecules rather than the surface of the nanoparticle, in many cases determine the outcomes of the nanoparticle interactions and fate in the body. Therefore, , the fundamental understanding of the structure/dynamics of a biomolecule (RNA)/ND system is essential for further development and refinement of novel ND based materials for biomedical applications.

In this work, we investigate the dynamics of hydrated and de-hydrated RNA molecules on ND surfaces relative to neat RNA by using quasi-elastic neutron scattering (QENS) and atomistic molecular dynamics (MD) simulations. Through these methods, we are able to distinguish the water dynamics from RNA dynamics at different length scales. Contrary to the generally held notion that nanoscale spatial heterogeneity at interfaces lead to correlated particle motions[13], thereby slowing down the dynamics, our results show faster RNA dynamics on ND surfaces compared to dry or neat RNA water solution within the temperature range investigated. We attribute the faster dynamics on ND surfaces to the breaking of confinement (de-confinement hereafter) of both the RNA and water molecules, a result of the triple phase coexistence of water/RNA/ND at the interfacial layer that is covered by a biomolecular corona on the surfaces of the ND. This is purely an entropic effect and can as such be fine tuned by chemical

functionalization of the ND surface, fundamentally altering the properties of the biomolecules on nanomaterial surfaces.

Results

The incoherent neutron scattering cross-section for hydrogen (protium) is at least 20 times larger than for other atoms in the biomolecule - ND system. This unique characteristic is exploited to capture the dynamics of the tRNA (transfer RNA) within the tRNA-ND-water system by replacing the regular hydration water H_2O with heavy water (D_2O), since the cross section of deuterium is ??? times less than that of protium. Here we compare three different samples, tRNA hydrated with D_2O (RNA/D_2O), dehydrated tRNA on ND (RNA/ND) and D_2O hydrated tRNA on a ND surface (RNA/ND/D_2O). In these samples, the majority of hydrogen atoms belongs to tRNA molecules, indicating that the measured QENS spectra solely represent the dynamics from the tRNA component. The measured normalized QENS spectra, namely, the self-dynamic structure factor $S(Q,\omega)$, is plotted on a log scale as function of energy transfer in Figure 1a. The broadening of the central peak from the resolution function is the result of quasi-elastic scattering of neutrons from hydrogen atoms in the sample. The broader the central peak, the faster is the dynamics of hydrogen atoms in the samples. The QENS spectra at Q= 1.1Å^{-1} (Q being the magnitude of the wave vector transfer in the scattering) are compared for three different samples at temperature T = 300K. As can be seen, the central peak of the RNA/ND/D_2O sample is broader than the other two samples, implying faster tRNA dynamics in the presence of the ND and D_2O.

The Fourier transform of $S(Q,\omega)$, the intermediate scattering function (ISF), $F_H(Q,t)$, is plotted in Figure 1b at three different Qs (Q= 0.5, 0.9 and 1.5Å^{-1}) at T = 300K. The ISF $F_H(Q,t)$, known as the particle-particle correlation function, is the key function to connect theoretical prediction, neutron scattering experimental data and MD simulation results (described in details later in this paper). We use an asymptotic expression (Supplementary Information, Equation 2)[14] derived from the most popular glass transition theory, mode coupling theory (MCT)[15-18], to fit our experimental $F_H(Q,t)$ in the time range from ps to ns. The solid lines in figure 1b represent the fitted curves. The tRNA within the RNA/ND/D_2O (blue symbols) sample has the fastest relaxation dynamics, at all scattering wavelengths, as suggested by the rapidly decaying $F_H(Q,t)$.

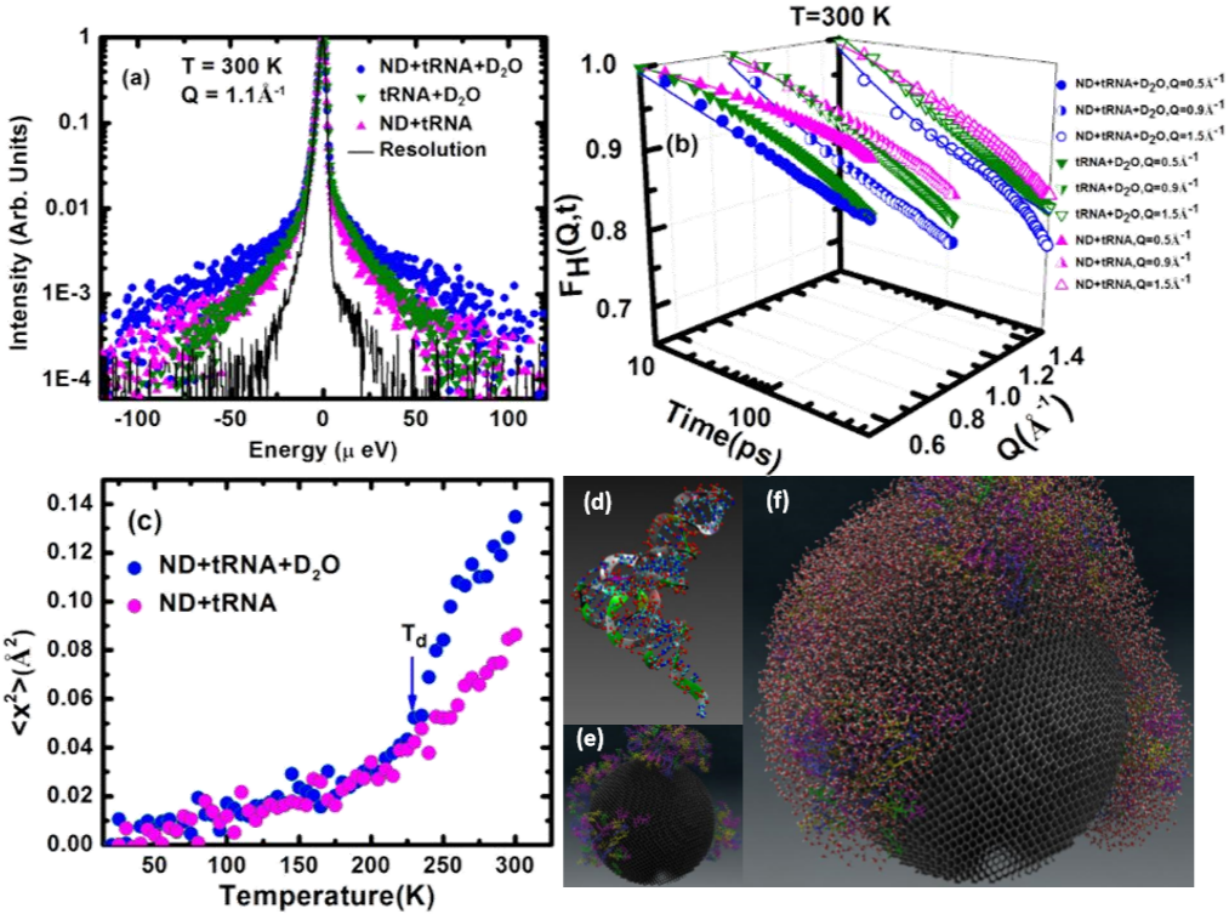

The mean square displacement (MSD) plotted as a function of temperature T is traditionally used

***Figure 1**: QENS data for RNA/ND/D_2O (blue), RNA/ND (magenta) and RNA/D_2O (green) systems. (a) Normalized QENS spectra S(Q,ω); and (b) Intermediate scattering function (ISF) at three Qs [Q= 0.5 (filled), 0.9 (half-closed) and 1.5 (open)$Å^{-1}$) for the three different systems. (c)Mean square displacement (MSD), $<x^2(T)>$, of RNA/ND/D_2O (blue) and RNA/ND (magenta) samples respectively. T_d represents "dynamic transition" temperature. There is no apparent dynamic transion observed in the RNA/ND sample; (d)-(f) Morphological cartoon from MD simulations of hydrated RNA molecules on a single ND, (d) a tRNA molecule at equilibrium, (e) eight RNA molecules adsorbed on the ND surface without water and (f) hydrated RNA molecules on the ND surface, representing the formation of corona by the RNA and water molecules on the ND surface. Some of water is also present forming a hydration shell around RNA.*

as an indicator of the flexibility (or 'softness') of the macromolecules , in our case, tRNA. At a given temperature, the steeper the slope of MSD vs T curve, the softer the macromolecule is[19].

The MSD is calculated through analysis of incoherent elastic scattering using the Debye Waller Factor, $S(Q,\omega=0) = \exp[-Q^2\langle x^2(T)\rangle]$, where $\langle x^2(T)\rangle$ is the MSD at temperature T. The MSD of hydrated and dehydrated tRNA with ND are plotted in Fig. 1(c). A sudden change in the slope of MSD at around 230K is observed in D_2O hydrated tRNA on the surface of ND, but not noticeable in the dehydrated sample. This inflection point is referred to the dynamic transition of biommacroolecules, which has also been observed in hydrated proteins[20,21] and hydrated tRNA[22], but not in their dry forms. Our observation shows that the activation of tRNA mobility occurs only in the hydrated state and this inflection is absent in dry sample[23,24]. In Figure 1d and 1e, we show a representative cartoon of a tRNA molecule and tRNA molecules on the surface of a ND. In Figure 1f, the MD snapshot shows the hydrated tRNA molecules on the surface of a single ND.

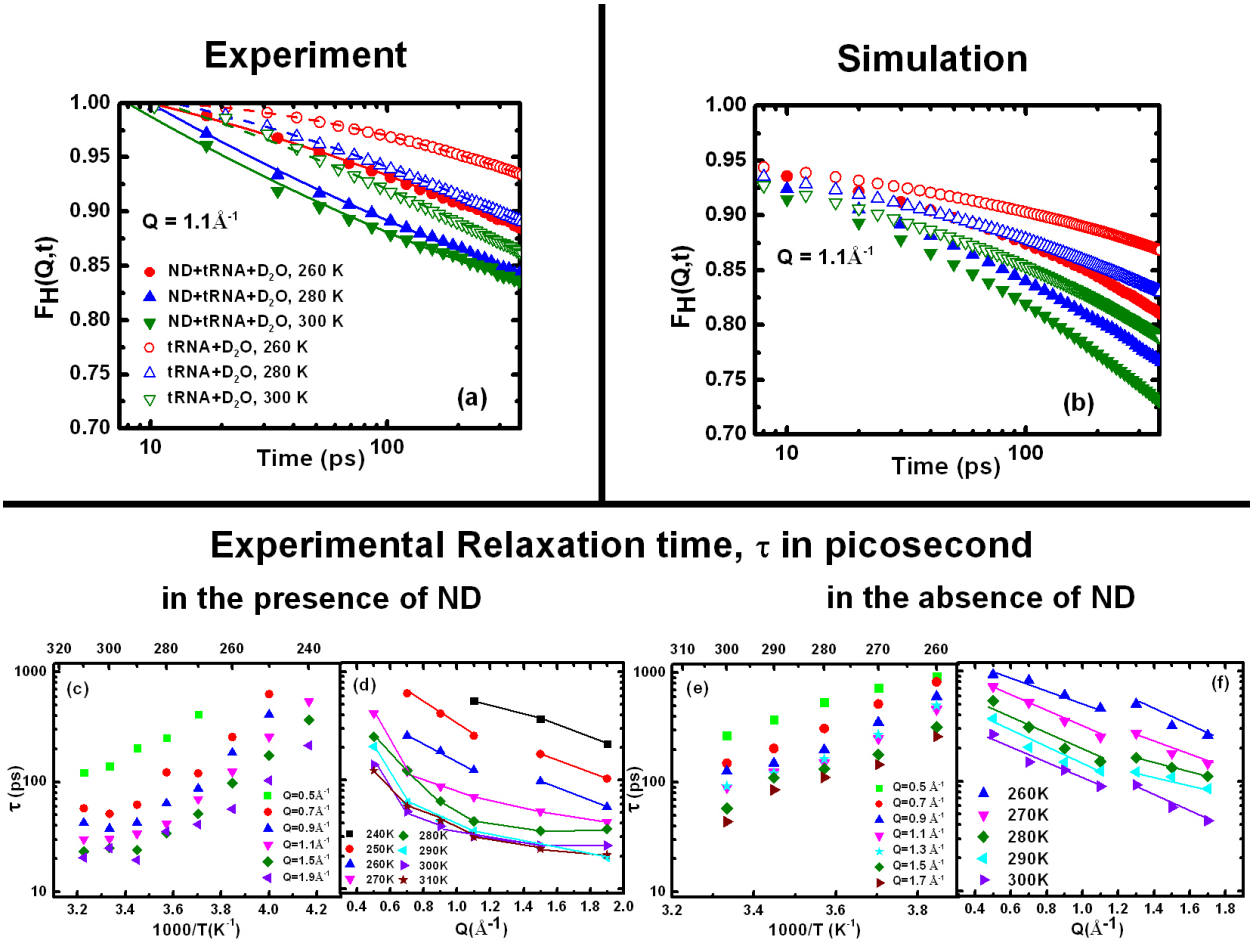

***Figure 2**: Comparison of experimental and MD simulation results of RNA/ND/D_2O and RNA/D_2O samples reveals a faster dynamics of RNA in the presence of ND. Experimental (a) and MD simulation (b) ISF of RNA/ND/D_2O and RNA/D_2O (samples at Q= 1.1$Å^{-1}$ and at T = 260K, 280K and 300K respectively). (c) Relaxation time as a function of inverse T at different Qs for RNA/ND/D_2O sample. (d) relaxation time as a function of Q at all temperatures for RNA/ND/D2O sample. (e) and (f) same as (c) and (d) respectively, but for RNA/D_2O sample*

Figure 2a shows the experimental ISF at Q = 1.1 $Å^{-1}$ and T = 260, 280 and 300K. Hydrated tRNA experiences faster dynamics in the presence of ND at 260, 280 and 300K. We estimated the relaxation time, τ, by taking the value at ISF=0.92[25] shown in supporting information Figure A2. The results are shown in Figure 2c-2f, for different temperatures and Q. Figure 2c-2d represent τ as a function of inverse T and Q for RNA/ND/D_2O, and figure 2e-2f represent the same for RNA/D_2O samples. At all Qs and temperatures, the relaxation time τ is 2-4 times faster in the presence of the ND (Figure 2c and 2e). While τ shows Vogel-Fulcher-Tammann (VFT) type decay (curves) in the presence of ND, an Arrhenius type decay (straight lines) is observed in the absence of ND, resembling a 'fragile' (Figure 2c) and 'strong' (Figure 2e) glassy behavior respectively. We refer this as 'jammed' state, as the system is not 'naturally glassy' but the sluggish motion of the RNA in the D_2O hydrated sample hinders its dynamics. Therfore, the 'fragile' and 'strong' jamming behavior is related to the 'weak' and 'strong' jammed state. The tRNA dynamics is largely influenced by this 'weakly jammed state' (Figure 2e) that leads to a considerable faster tRNA dynamics in the presence of ND. In Figure 2d and 2f, the scaling shows a strongier Q-dependence of τ for tDNA compared to the smaller macromolecular counterparts[26-29]. In macromolecules[26-29], the Q-dependence in the Q-range < $1Å^{-1}$ follows a power law, $\tau(Q) \sim Q^{-2/\beta}$, where β is the stretching exponent ranging between 0.4-0.65. Figure 2d and 2f show a much slower decay (fit not shown here) with β ranging from 0.32-38 and 0.26-32 for RNA/ND/D_2O and RNA/D_2O respectively. Therefore, β for both the cases are smaller than typical polymers, i.e. a higher exponent for tRNA, representing a slower tRNA dynamics compared to typical polymers in both cases. As a general tendency, the presence of ND should slow down the motion of RNA as has been observed on a silica surface[30]. In our study, an 'enhancement' of the dynamics of the strongly interacting hydrated RNA is observed on ND surface. This counterintuitive phenomenon of faster dynamics on an obstructive surface is

critical to the motion of large biomolecules in the presence of a functionalized nanoparticle, in this case ND. In Figure 2f, we also noticed a step jump of τ within the Q-range 1.1-1.3Å^{-1} that relates to 4.8 to 5.7Å length scale. tRNA motion is faster at > 5.7Å length scales and slower at the shorter length scales. The same is observed until T = 260K in RNA/ND/D_2O case (Figure 2d) but with a kink-jump at Q = 1.1Å^{-1}. Therefore, the molecular motions of the hydrated only tRNA are not homogeneous at all the length scales; however the same gives a molecular scale intrinsic non-exponential relaxation in the presence of ND. This critical feature of tRNA dynamics can be related to heterogeneous dynamics of the large biomolecules on two different length scales in the absence of ND[13,31].

To further investigate the underlying mechanism of the tRNA motion, we carried out an all-atom MD simulations of the hydrated RNA in the presence or absence of ND. It has already been established[32] that tRNA can be represented by hammerhead RNA to accurately explain the neutron scattering results from tRNA[14]. We also used hammerhead RNA in the presence and absence of ND in our simulations[33] with experimental parameters. The simulation results are shown in Figure 2b. The simulated ISFs also show a faster dynamics of the D_2O hydrated RNA on ND surface and hence are in qualitative agreement with experimental results.

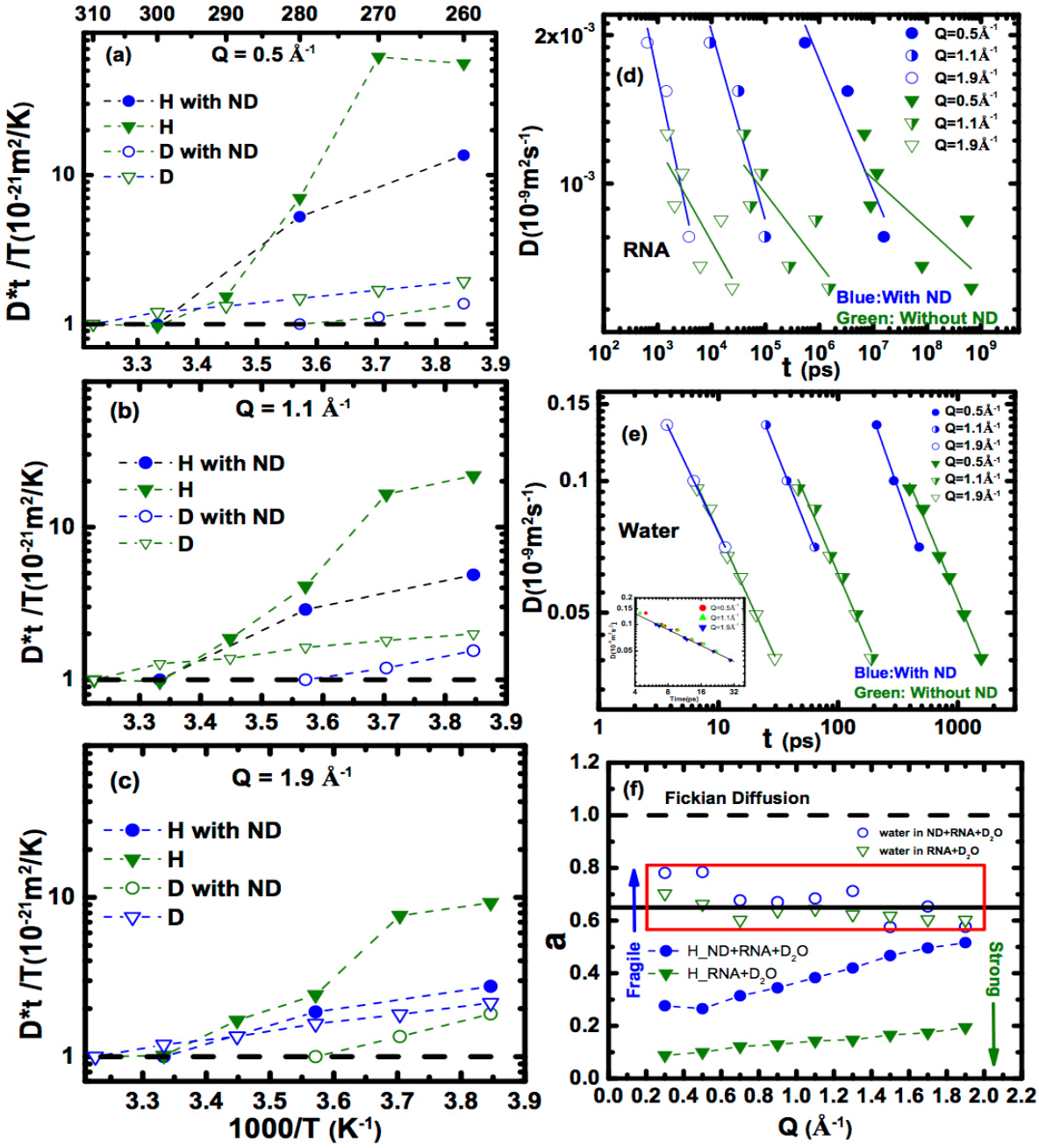
(a) Q = 0.5 Å-1
H with ND
H
D with ND
D
D*t /T(10-21m2/K)
(b) Q = 1.1 Å-1
(c) Q = 1.9 Å-1
1000/T (K-1)
(d)
RNA
Blue:With ND
Green: Without ND
D(10-9m2s-1)
t (ps)
(e)
Water
(f) Fickian Diffusion
water in ND+RNA+D2O
water in RNA+D2O
H_ND+RNA+D2O
H_RNA+D2O
Fragile
Strong
a
Q (Å-1)

***Figure 3**: Comparison of Protium of RNA (HRNA) and Deuterium of Water (D_2O) scaling behavior and Stokes-Einstein Relation (SER) from diffusion constant (D) and relaxation time (τ) obtained from our simulation. The deuterated water dynamics cannot be observed from experiments, therefore, the only way the essential water dynamics canbe understood is from MD simulation as shown in this figure. Left panel: Dτ/T as a function of inverse temperature. Filled blue circles and filled green triangles represent HRNA of RNA/ND/D_2O and RNA/D_2O samples respectively. Empty blue circles and empty triangles represent D_2O of water for RNA/ND/D_2O and RNA/D_2O samples respectively. (a) SER for The Stokes-Einstein Relation (SER) for Q = 0.5 representing a strong influence of HRNA and D_2O for both the samples. All the cases, SER is broken. (b)-(c) same as (a) but with smaller exponent with higher Qs. Water dynamics follows remarkably the same scaling law for all the Q values. (d)-(f) Calculation of scaling exponent from $D \sim t^{-\alpha}$. (d) D as a function of t for HRNA at 3 different Q values, 0.5 (filled), 1.1 (half-filled) and 1.9 (open) respectively. The blue circle and green down triangles represent with (RNA/ND/D_2O) and without ND (RNA/D_2O) samples respectively. (e) Same as (d) for water (D_2O). The inset shows a master curve for water dynamics that follows same scaling behavior for all the parameter ranges and for different samples. (f) Scaling exponent, α as a function of Q representing the values at different length scales. The α values are derived from (d) and (e) using a non-linear least-squares Marquardt-Lavenberg algorithm. The red blocked region is drawn to focus on the water (D_2O) α-value ranges. The dashed-line at 1.0 represents normal Fickian diffusion. Higher 'fragility' is represented by smaller α-values, whereas larger a-values represent strong 'glassy' dynamics. The water shows very weak SER violation with higher 'fragility'. However, the RNA shows quite small exponent representing stronger SER violation that we define as 'jammed state' for the RNA.*

In Figure 3, we present the scaling analysis of the simulated transport coefficients, which provides a better understanding of the critical dynamics of hydrated RNA on ND. To answer, "*why does RNA exhibit a faster relaxation dynamics on a ND surface?*", as observed in our QENS experiments, we plotted the standard numerical quantity for the validation of Stokes-Einstein Relation (SER), Dτ/T, as a function of 1000/T in the left panel (Figure 3a, 3b and 3c) and D (where D is diffusion constant) as a function of t on the right panel (Figure 3d and 3e) at short, medium and long length scales, Q = 0.5, 1.1 and 1.9$Å^{-1}$ respectively. Highly mobile molecules move through regions of less mobile molecules, which has consequences in the validity of SER[34,35] given by, $D \sim t^{-\alpha}$, where 'α' is the exponent. For α = 1.0, the dynamics follow normal Fickian diffusion i.e., no violation of SER. To follow SER, Dτ/T must be constant with 1/T. In Figure 3a-3c, the normalized Dτ/T (normalized to the highest temperature value) shows a large deviation of the RNA from unity (black dashed line at 1.0) without ND. However the presence of ND reduces the deviation. Therefore, the RNA shows a strong violation of SER without ND and a weaker violation with ND. Water, on the other hand, shows a smaller

deviation representing the weakest violation of SER. The violation of SER is related to the heterogeneous dynamics (HD) of the molecule that is associated with 'highly mobile' and 'immobile' motion. The stronger SER violation represents stronger heterogeneity in the dynamics leading to a weaker molecular relaxation as in the case of neat RNA. On the other hand, a weaker SER violation leads to a faster dynamics as is observed in the presence of ND. The same was confirmed by the experiments in Figure 2a and 2c-2f. As the length scale decreases (from Figure 3a to 3c) the absolute value of $D\tau/T$ reduces, indicating a reduction of heterogeneity in molecular motion. Heterogeneous dynamics is well established for biomolecules in living systems[13,36,37] and the observed HD falls under the generalized characteristic motion of bio-macromolecules. The significance of the MD simulation lies in the critical analysis of the D_2O dynamics that cannot be detected otherwise by neutron experiments. To show the SER breakdown, $D \sim t^{-\alpha}$, in a rigorous way, we plotted D versus τ in Figure 3d and 3e. From Figure 3d, RNA dynamics in the presence of ND (blue circles) shows faster dynamics than without ND (green triangles). The plots show two different scaling behaviors (Figure 3d). The green symbols scales with α = 0.1-0.2 whereas the blue symbols scales with α = 0.27-0.52. Figure 3e shows scaling behavior of water varying from α = 0.6-0.66 without ND (green symbols) to 0.58-0.78 with ND (blue symbols). Therefore, the hydrated RNA shows a 'stronger' jamming behavior without ND (lower exponent values). Such a strong and weak violation of SER corresponds to strong and weak coupling in biomolecules which is consistent with the idea that decoupling is related to heterogeneous dynamics that is absolutely important for the motion of fragile liquids[38,39], in this case the motion of the RNA on the ND surface. The line shown in the inset of Figure 3e represents the universal scaling dynamics of D_2O with a universal scaling exponent α = 0.6, showing a universal water fragility with our without ND although the diffusion coefficient is higher in the former case. The α values are plotted in Figure 3f. $\alpha \sim 1.0$ and far from 1.0 represent fragile and strong liquid behavior respectively. α shows small differences for water and close to 1.0 within the dashed region, therefore, 'fragile'. However, there is a large difference in RNA α with or without ND. With or without ND, α for RNA varies from 0.1-0.2 to 0.3-0.5 representing a strong and fragile jammed state. Therefore, the RNA motion is restricted without ND, as evident by a slower decay in Figure 1b.

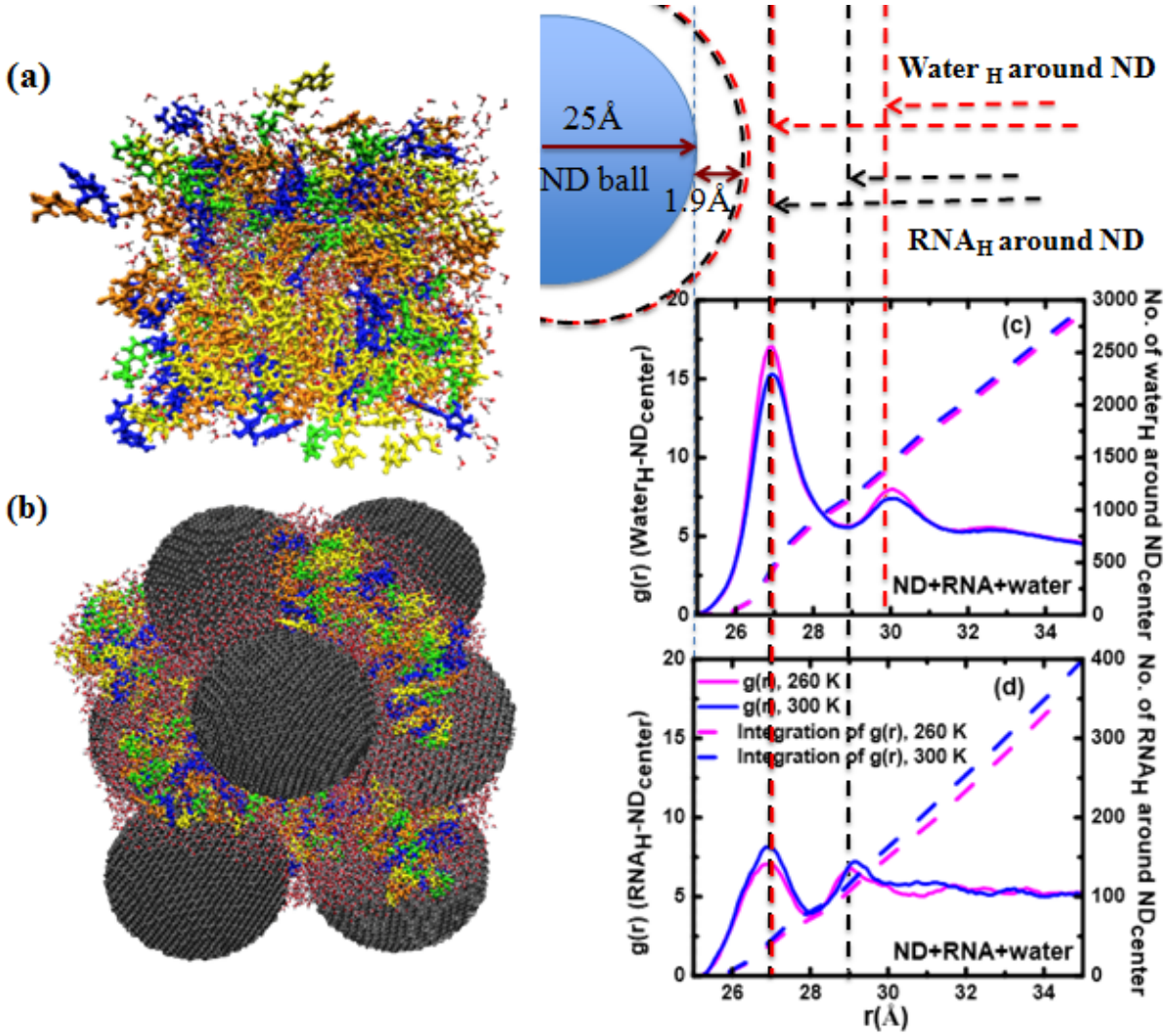
(a)
(b)
25Å
ND ball
1.9Å
Water H around ND
RNAH around ND
(c)
g(r) (WaterH-NDcenter)
No. of waterH around NDcenter
ND+RNA+water
(d)
g(r), 260 K
g(r), 300 K
Integration pf g(r), 260 K
Integration pf g(r), 300 K
g(r) (RNAH-NDcenter)
No. of RNAH around NDcenter
ND+RNA+water
r(Å)

***Figure 4**: Structural analysis of the RNA/ND/D_2O sample using MD simulations. (a) Snapshot at the end of simulation for RNA/D_2O system. (b) Same for RNA/ND/D_2O sample. Each simulation box contains eight RNA molecules and eight nanodiamonds. The water molecules are represented by red (oxygen) and silver (hydrogen) colors. Right top panel: a cartoon illustrating the average displacement of the hydrogen atoms of water (red) and RNA (black) molecules from the ND surface. (c) and (d) Radial distribution function, g(r) on the left axis and coordination number around ND at two temperatures T = 260K (magenta) and 300K (blue) respectively. The dashed lines represent number of molecules (right axis) for the respective temperatures. Note that the radius of ND in our simulation is 2.5nm (25Å), therefore g(r) are plotted starting from 25Å.*

Figure 4a and 4b show MD simulation snapshots of the RNA/D_2O and RNA/ND/D_2O samples, respectively. The radial distribution function, g(r), of water hydrogen (H) and RNA hydrogen (H) from ND surface is plotted in Figure 4c-4d and extends to r=10Å. The corresponding number of water molecules is shown on the right. In Figure 4c and d, water and RNA both are observed on the ND surface in RNA/ND/D2O sample at 260 and 300K. However, water profusely hydrates the ND surface, (~500 molecules Figure 4c) compared to RNA (~40 molecules Figure 4d) on the ND surface at 27Å. While the large number of water molecules surrounds the first layer of ND surface, the number of water molecule around the RNA is negligibly low (~2-3, see SI Figure E(a)). Also, the g(r) peak, probability of finding a water H near ND surface, is twice as high as the RNA_H near ND surface or a $water_H$ around RNA_H. The result shows similar number of $water_H$ around RNA_H in the absence of ND (SI figure E(b)) however with smaller g(r) peak. Considering the natural $water_H$ distribution around RNA_H without any surface interactions, the presence of hydrophilic ND surface shows ten times (8.0 in SI figure E(a) compared to 0.8 in SI Figure E(b)) higher probability of finding $water_H$ around RNA. The presence of large number of water on ND surface and higher peak in g(r) of RNA_H on the surface is possible only if there is an interfacial layer between the ND and the RNA that makes water accessible to both the RNA and the ND surfaces while keeping the ND-corona[12] shape. In Figure 4c, g(r) of water around a ND center shows three peaks at 27Å, at 30Å and 32.5Å. The peaks for the RNA are at 26.9, 29 and 31.5 Å respectively. While the first peak of RNA and $water_H$ are located at roughly the same

position (1.9 Å), the second and third peaks differ by ~1Å. This represents de-confinement of RNA on the far side of the ND. Furthermore, the otherwise attractive interaction between RNA and ND is weakened due to a high-density interfacial water layer. Moreover, it was observed in Figure 3 that the RNA_H violates SER with a weaker heterogeneity on ND surface compared to a freestanding RNA leading to a faster RNA motion on ND surface. The weaker heterogeneous dynamics of the RNA leading to their faster dynamics and at the same time same number of water molecule surround the RNA with or without ND. This can only be possible if the interfacial water layer is also 'de-confining' the RNA from ND thereby giving rise to faster dynamics and forming an interfacial layer. *The existence of large number of water on the ND surface and the interfacial water layer is a result of the combination of de-confinement of RNA and a strong hydrophilic interaction of water with the ND surface.*

Conclusion

We conclude that both structural and dynamics factors are involved in the observed RNA dynamics on the ND surface. RNA exhibits a weaker heterogeneous dynamics on a ND surface than a neat hydrated RNA. The weaker heterogeneity is facilitated by a weaker SER violation leading to a 'fragile' jammed state compared to freestanding RNA with a 'strong' jammed states facilitated by a strong SER violation. These results are strinkingly different in comparison to previous experimental observations on another set of biomolecules on silica surface[30], where it was argued that the adsorption of biomolecules not only decreased the flexibility but simultaneously modified the mobility of residues and dynamics upon surface interaction. Structurally, water molecules form an interfacial layer between RNA and ND with a high probability of water molecule between RNA and the ND surface. This gives rise to a de-confinement of RNA molecule with weaker heterogeneous dynamics. A de-confined RNA molecule leads to a faster relaxation dynamics consistent with SER violation. The water molecule, on the other hand, shows 'weak' SER violation and follows a universal scaling law.

Hydrated RNA exhibits faster dynamics on a ND surface compared to a freestanding case in both QENS and MD simulations. These observations prompt us to revisit the RNA dynamics in RNA-biomolecule composites. The fragility of the RNA is suppressed in the absence of ND leading to

a higher order breakdown of SER. The SER breakdown is weaker in the presence of ND. At the same time, the water molecule from the hydrated RNA is released on hydrophilic ND surface to form an interfacial water layer leading to a de-confined RNA and hence faster dynamics. The simulations are in 'qualitative' agreement with the experimental results. The techniques used here allow a precise determination and detailed explanation of RNA dynamics and structures in biomacromolecules nanocomposites. The combination of faster dynamics and de-confinement of RNA on ND surface provides unique opportunities to enhance the drug-delivery mechanisms in RNA nanotechnology by introducing a small portion of non-toxic, highly functionalizable ND. ND can also be integrated with other hydrophilic biomolecules and enhance the properties of materials for bactericidal activity, drug-delivery and even for treating viral diseases.

Acknowledgements

This work was supported by the U.S. Department of Energy (DoE), Office of Basic Energy Sciences, Materials Science and Engineering Division. This research used resources of the Oak Ridge Leadership Computing Facility at the Oak Ridge National Laboratory, which is supported by the Office of Science of the U.S. Department of Energy under Contract DE-AC05-00OR22725. Research by M.G and J.M.B is supported by the Center for Accelerated Materials Modeling (CAMM) funded by the U.S. DoE, BES, MSED. BGS and PG acknowledge work performed at the Center for Nanophase Materials Sciences, a DOE Office of Science User Facility. This research used resources of the Oak Ridge Leadership Computing Facility at the Oak Ridge National Laboratory, which is supported by the Office of Science of the U.S. Department of Energy under Contract No. DE-AC05-00OR22725 and also National Energy Research Scientific Computing Center, a DOE Office of Science User Facility supported by the Office of Science of the U.S. Department of Energy under Contract No. DE-AC02-05CH11231.

Author Contribution

Xiang-qiang Chu and Panchapakesan Ganesh conceived the idea for performing this study. Xiang-qiang Chu conceptually designed and started the experiments and engaged in the collaboration with different laboratories. Debsindhu Bhowmik performed experiments, data

analysis and helped write the paper. Gurpreet K. Dhindsa performed QENS experiments and data analysis and major plotting. Vadym N. Mochalin and Yury Gogotsi prepared the ND samples. Hugh O'Neill and Eugene Mamontov helped with the QENS experiments. Monojoy Goswami helped set-up the simulations, performed the scaling analysis and helped interpret the experimental results based on this analysis and simulations. All authors contributed to writing the paper.

Materials and Methods

NDs (radius ~2.5nm) were prepared with detonation technique[10] and were placed inside a vacuum oven to remove most of water molecules adsorbed on ND surfaces. tRNA was bought from Sigma Aldrich and was used without further purification. The hydrated sample was prepared by adsorbing 0.03 g of tRNA on 0.33g of dry ND surface, and then hydrated with 0.06g of D_2O. The dry sample was prepared by directly adsorbing tRNA on ND surfaces without hydration process. For D_2O hydrated tRNA sample without ND, we used data from our previous experiment where tRNA hydration level was h = 0.5(g of D_2O/g of tRNA)[14].

The QENS experiments were performed on a nearbackscattering spectrometer BASIS [E. Mamontov 2011] at the Spallation Neutron Source (SNS) at Oak Ridge National Laboratory (ORNL). The details of the neutron scattering experiments are described in the SI.

***Simulation Methodology*:** MD Simulations are performed on hydrated RNA systems both with and without the presence of ND. The initial coordinates for hammerhead (RNA) were taken from the protein data bank (PDB: 299D). This RNA model has already been used to explain and match the neutron scattering results from tRNA[40]. We extended this idea by using MD simulations of D_2O hydrated RNA in the presence and absence of ND (Figure 4(a) and 4(b)), matching the experimental conditions. The hydration level in the D_2O hydrated RNA without ND, is kept at par with the experiments i.e., h=0.5 (g D_2O/g of RNA). Initially for the simpler of the two systems i.e., without ND, a single RNA is placed into a pre-equilibrated box of water eliminating the overlapping water molecules and subsequently replicating into 8 clones. Furthermore, adding the required number of sodium ions neutralizes the charge in the system. Also each of the eight RNA molecules, the ions and water are rotated by a random angle around a randomly chosen principal axis. In case of the system with ND, eight 2.5nm (radius) ND spheres are prepared to mimic the experimental conditions. The 8 RNAs and 10464 water molecules are placed around the eight 2.5nm radius NDs (containing a total of 92320 carbon atoms) matching the experimental RNA, water and ND ratio. The required numbers of sodium ions are then added to make the system charge neutralized. Simulations are performed on both

systems using the CHARMM-27 protein nucleic acid force field[41] and TIP3P[42] water model using NAMD[33]. We built a ND particle of of carbon atoms positioned according structure of diamond and used Lennard-Jones (LJ) parameters from available literature to keep it hydrophilic. In our work the σ and ε parameters of the LJ potential, representing the interactions between the non-bonded carbon atoms are calculated from the parameters of graphite and carbon nanotubes[43]. The mixing of interactions and bonds are done by applying the Lorentz-Berthelot rule. The surface of the system satisfies the condition of hydrophilicity, which requires the size of the solvent particles to be smaller than that of solute particles and the strength of solvent-solvent intermolecular interactions to be weaker than that of solute-solvent interactions[44]. Here the solute is nanodiamond and the solvent is water. The deuteration of water is done during analysis using nMoldyn[45]. This is a standard procedure used for simulated data in order to match neutron experiments data[45,46]. The only difference is that deuteration increases the viscosity by 1.23 (at 298K) compared to water. So we see $R_{min/2\ CC} = 1.92Å > R_{min/2\ HH} = 0.2245Å$ and $R_{min/2\ CC} = 1.92Å > R_{min/2\ OO} = 1.7682Å$ (R_{min} is the distance where the potential attains the minimum). In other relevant work, Sendner et al.[47] showed how hydrophobicty/hydrophilicity varies with the interaction energy while keeping the size unchanged. In that work the interaction energy (ε_{CO}) between carbon and oxygen atoms was tuned between 0.026Kcal/mol and 0.171Kcal/mol, with greater hydrophobic behavior corresponding to the decreased interaction energy. In our simulation, ε_{CO} = 0.138Kcal/mol, ε_{CH} = 0.077Kcal/mol and ε_{OO} = -0.15210Kcal/mol, ε_{HH} = -0.04600Kcal/mol. Obviously this made the ND surface more hydrophilic in nature. Periodic boundary conditions are used to determine the long-range electrostatic interactions. The short-range interactions are calculated within the cut off 12Å and Particle Mesh Ewald (PME) is used to evaluate the long-range interactions. Prior to data collection runs, energy of the systems was minimized and the systems were equilibrated for 6ns in the NPT ensemble at five different temperatures, T = 260K, 270K, 280K, 290K and 300 K. The RMSD plots of two different Systems at different temperatures are presented in Supplementary Information, Figure C. After equilibration, simulations are carried out for another 5ns at each temperature with time step of 1fs. The subsequent analyses of the dynamics were performed by nMoldyn[45].

(*Word Count: Materials and Methods - 888*)

References:

[reference count: 47 (<50)]

1 Guo, P. The emerging field of RNA nanotechnology. *Nature nanotechnology* **5**, 833-842, doi:10.1038/nnano.2010.231 (2010).

2 Mochalin, V. N., Shenderova, O., Ho, D. & Gogotsi, Y. The properties and applications of nanodiamonds. *Nature nanotechnology* **7**, 11-23, doi:10.1038/nnano.2011.209 (2012).

3 Aldaye, F. a., Palmer, A. L. & Sleiman, H. F. Assembling materials with DNA as the guide. *Science* **321**, 1795-1799, doi:10.1126/science.1154533 (2008).

4 Seeman, N. C. Nanomaterials based on DNA. *Annual review of biochemistry* **79**, 65-87, doi:10.1146/annurev-biochem-060308-102244 (2010).

5 Liu, K.-K. *et al.* Covalent linkage of nanodiamond-paclitaxel for drug delivery and cancer therapy. *Nanotechnology* **21**, 315106, doi:10.1088/0957-4484/21/31/315106 (2010).

6 Wehling, J., Dringen, R., Zare, R. N., Maas, M. & Rezwan, K. Bactericidal activity of partially oxidized nanodiamonds. *ACS Nano* **8**, 6475-6483, doi:10.1021/nn502230m (2014).

7 Wang, J., Hu, Z., Xu, J. & Zhao, Y. Therapeutic applications of low-toxicity spherical nanocarbon materials. *NPG Asia Materials* **6**, e84 (2014).

8 Zhou, G., Lelkes, P. I., Hill, C., Gogotsi, Y. & Mochalin, V. Functionalized Nanodiamond Reinforced Bioplymers. **1** (2012).

9 Chung, P. H., Perevedentseva, E., Tu, J. S., Chang, C. C. & Cheng, C. L. Spectroscopic study of bio-functionalized nanodiamonds. *Diamond and Related Materials* **15**, 622-625, doi:10.1016/j.diamond.2005.11.019 (2006).

10 Kharlamova, M. V. *et al.* Adsorption of proteins in channels of carbon nanotubes: Effect of surface chemistry. *Materials Express* **3**, 1-10, doi:10.1166/mex.2013.1102 (2013).

11 Xing, Y. & Dai, L. Nanodiamonds for nanomedicine Review. *Nanomedicine* **4**, 207-218, doi:10.2217/17435889.4.2.207 (2009).

12 Monopoli, M. P., Åberg, C., Salvati, A. & Dawson, K. A. Biomolecular coronas provide the biological identity of nanosized materials. *Nature Nanotechnology* **7**, 779, doi:10.1038/NNANO.2012.207 (2012).

13 Pronk, S., Lindahl, E. & Kasson, P. M. Dynamic heterogeneity controls diffusion and viscosity near biological interfaces. *Nature communications* **5**, 3034, doi:10.1038/ncomms4034 (2014).

14 Chu, X.-q., Mamontov, E., O'Neill, H. & Zhang, Q. Temperature Dependence of Logarithmic-like Relaxational Dynamics of Hydrated tRNA. *The Journal of Physical Chemistry Letters* **4**, 936-942, doi:10.1021/jz400128u (2013).

15 Sciortino, F., Tartaglia, P. & Zaccarelli, E. Evidence of a higher-order singularity in dense short-ranged attractive colloids. *Physical review letters* **91**, 268301, doi:10.1103/PhysRevLett.91.268301 (2003).

16 Götze, W. & Sperl, M. Logarithmic relaxation in glass-forming systems. *Physical Review E - Statistical, Nonlinear, and Soft Matter Physics* **66**, 011405, doi:10.1103/PhysRevE.66.011405 (2002).
17 Lagi, M., Baglioni, P. & Chen, S.-H. Logarithmic Decay in Single-Particle Relaxation of Hydrated Lysozyme Powder. *Physical Review Letters* **103**, 108102, doi:10.1103/PhysRevLett.103.108102 (2009).
18 Chu, X.-q. *et al.* Experimental evidence of logarithmic relaxation in single-particle dynamics of hydrated protein molecules. *Soft Matter* **6**, 2623, doi:10.1039/c002602f (2010).
19 Zaccai, G. How soft is a protein? A protein dynamics force constant measured by neutron scattering. *Science (New York, N.Y.)* **288**, 1604-1607, doi:10.1126/science.288.5471.1604 (2000).
20 Roh, J. H. *et al.* Influence of hydration on the dynamics of lysozyme. *Biophysical journal* **91**, 2573-2588, doi:10.1529/biophysj.106.082214 (2006).
21 Roh, J. H. *et al.* Onsets of anharmonicity in protein dynamics. *Physical Review Letters* **95**, 1-4, doi:10.1103/PhysRevLett.95.038101 (2005).
22 Nickels, J. D., Curtis, J. E., O'Neill, H. & Sokolov, A. P. Role of methyl groups in dynamics and evolution of biomolecules. *Journal of Biological Physics* **38**, 497-505, doi:10.1007/s10867-012-9268-6 (2012).
23 Caliskan, G. *et al.* Dynamic transition in tRNA is solvent induced. *Journal of the American Chemical Society* **128**, 32-33, doi:10.1021/ja056444i (2006).
24 Dhindsa, G. K., Tyagi, M. & Chu, X.-Q. Temperature-Dependent Dynamics of Dry and Hydrated β-Casein Studied by Quasielastic Neutron Scattering. *The journal of physical chemistry. B*, doi:10.1021/jp504548w (2014).
25 Chu, X.-q. *et al.* Dynamic behavior of oligomeric inorganic pyrophosphatase explored by quasielastic neutron scattering. *The journal of physical chemistry. B* **116**, 9917-9921, doi:10.1021/jp303127w (2012).
26 Colmenero, J., Alegria, A., Arbe, A. & Frick, B. Correlation between Non-Debye Behavior and Q Behavior of the α Relaxation in Glass-Forming Polymeric Systems. *Physical Review Letters* **69**, 478-481, doi:10.1103/PhysRevLett.69.478 (1992).
27 Colmenero, J., Arbe, A. & Alegria, A. Crossover from Debye to Non-Debye Dynamical Behavior of the α Relaxation Observed by Quasielastic Neutron Scattering in a Glass-Forming Polymer. *Physical Review Letters* **71**, 2603-2606, doi:10.1103/PhysRevLett.71.2603 (1993).
28 Colmenero, J. *et al.* Crossover from Independent to Cooperative Segmental Dynamics in Polymers: Experimental Realization in Poly(Vinyl Chloride). *Physical Review Letters* **78**, 1928-1931, doi:10.1103/PhysRevLett.78.1928 (1997).
29 Ngai, K. L., Colmenero, J., Alegría, A. & Arbe, A. Interpretation of Anomalous Momentum Transfer Dependences of Local Chain Motion of Polymers Observed by Quasielastic Incoherent Neutron Scattering Esperiments. *Macromolecules* **25**, 6727-6729, doi:10.1021/ma00050a056 (1992).
30 Devineau, S. *et al.* Myoglobin on silica: A case study of the impact of adsorption on protein structure and dynamics. *Langmuir* **29**, 13465-13472, doi:10.1021/la4035479 (2013).

31 Chandler, D. & Garrahan, J. P. Dynamics on the way to forming glass: bubbles in space-time. *Annual review of physical chemistry* **61**, 191-217, doi:10.1146/annurev.physchem.040808.090405 (2010).
32 Zhang, H., Khodadadi, S., Fiedler, S. L. & Curtis, J. E. Role of Water and Ions on the Dynamical Transition of RNA. *The Journal of Physical Chemistry Letters* **4**, 3325-3329, doi:10.1021/jz401406c (2013).
33 Phillips, J. C. *et al.* Stable Molecular Dynamics with NAMD. *Journal of Computational Chemistry* **26**, 1781-1802, doi:10.1002/jcc.20289 (2005).
34 Einstein, A. Über die von der molekularkinetischen Theorie der Wärme geforderte Bewegung von in ruhenden Flüssigkeiten suspendierten Teilchen. *Annalen der Physic* **322**, 549, doi:10.1002/andp.19053220806 (1905).
35 Stokes, G. G. On the Effect of the Internal Friction of Fluids on the Motion of Pendulums. *Transactions of the Cambridge Philosophical Society* **9**, 8 (1851).
36 Garrahan, J. P. Dynamic heterogeneity comes to life. *Proceedings of the National Academy of Sciences of the United States of America* **108**, 4701-4702, doi:10.1073/pnas.1101436108 (2011).
37 Angelini, T. E. *et al.* Glass-like dynamics of collective cell migration. *Proceedings of the National Academy of Sciences of the United States of America* **108**, 4714-4719, doi:10.1073/pnas.1010059108 (2011).
38 Berthier, L. & Biroli, G. Theoretical perspective on the glass transition and amorphous materials. *Reviews of Modern Physics* **83**, 587-645, doi:10.1103/RevModPhys.83.587 (2011).
39 Ediger, M. D. SPATIALLY HETEROGENEOUS DYNAMICS IN SUPERCOOLED LIQUIDS. *Annu. Rev. Phys. Chem.* **51**, 99-128, doi:10.1146/annurev.physchem.51.1.99 (2000).
40 Shi, Z., Debenedetti, P. G. & Stillinger, F. H. Relaxation processes in liquids: Variations on a theme by Stokes and Einstein. *Journal of Chemical Physics* **138**, 12A526, doi:10.1063/1.4775741 (2013).
41 Mackerell, A. D. & Banavali, N. K. All-Atom Empirical Force Field for Nucleic Acids: II. Application to Molecular Dynamics Simulations of DNA and RNA in Solution. *Journal of Computational Chemistry* **21**, 105-120, doi:10.1002/(SICI)1096-987X(20000130)21:2<105::AID-JCC3>3.0.CO;2-P (2000).
42 Jorgensen, W. L., Chandrasekhar, J., Madura, J. D., Impey, R. W. & Klein, M. L. Comparison of simple potential functions for simulating liquid water. *The Journal of Chemical Physics* **79**, 926, doi:10.1063/1.445869 (1983).
43 Werder, T. *et al.* On the Water - Carbon Interaction for Use in Molecular Dynamics Simulations of Graphite and Carbon Nanotubes. *Journal of Physical Chemistry B* **107**, 1345-1352, doi:10.1021/jp0268112 (2003).
44 Ishizaki, M., Tanaka, H. & Koga, K. Hydrophobicity in Lennard-Jones solutions. *Physical chemistry chemical physics : PCCP* **13**, 2328-2334, doi:10.1039/c0cp01767a (2011).
45 T., R., K., M., K., H. & Kneller, G. R. nMoldyn : A Program Package for a Neutron Scattering. *Journal of Computational Chemistry* **24**, 657-667 (2003).
46 Bhowmik, D. *et al.* Aqueous solutions of tetraalkylammonium halides: ion hydration, dynamics and ion-ion interactions in light of steric effects. *Physical chemistry chemical physics : PCCP* **16**, 13447-13457, doi:10.1039/c4cp01164c (2014).

47 Sendner, C., Horinek, D., Bocquet, L. & Netz, R. R. Interfacial water at hydrophobic and hydrophilic surfaces: slip, viscosity, and diffusion. *Langmuir : the ACS journal of surfaces and colloids* **25**, 10768-10781, doi:10.1021/la901314b (2009).